

Surface Current Analysis from High Frequency Radar Measurement off the Coast of Yantai, China

X. Zheng, G. Bruss & R. Mayerle

University of Kiel, Research and Technology Centre Westcoast, Germany

C. Tang

Yantai Institute of Coastal Zone Research, Chinese Academy of Sciences, China

ABSTRACT: A land based high frequency (HF) radar system was installed at the coast of the Yellow Sea, about 35 km east of the city of Yantai in China. The system measures surface currents and waves operationally since July 2013. The HF radar is part of a nowcasting modeling system currently under development for the north coast of the Shandong Peninsula. The data has been used to improve the understanding of the hydrodynamic processes and for calibration and validation of a coupled flow and wave model. From July 23 to September 10, 2013, a bottom-mounted ADCP was deployed within the coverage area for assessing the accuracy of the radar. Comparisons between the current velocities measured by the two instruments showed good agreement. The analysis of the radar data helped to identify the relevant processes responsible for the characteristic current patterns within the area of interest. Spectral analysis of the surface current velocities and local wind data showed that tides and large scale circulations within the Bohai Sea and Yellow Sea are the dominating driving forces of the local surface currents in the area. Harmonic analysis was performed to characterize the tidal currents in the region. Low pass filtering revealed the presence of a longshore current of low frequency. A detail description of the applied methods and filtering techniques is presented.

Keywords: *HF radar, ADCP, Ocean surface current, Spectrum analysis*

1 INTRODUCTION

Coastal areas around the world are highly populated and intensively used. Their proper management is of vital importance and there is an increasing need to monitor such environments. Regarding marine measurements a distinction can be made between in-situ and remote sensing techniques. Conventional in-situ instruments such as tide gauges, wave buoys or stationary ADCPs present reliable accuracies but are usually limited in spatial coverage due to high costs and time-consuming deployments. Remote sensing observations can cover larger areas and land based systems such as high frequency (HF) radars are installed and maintained at comparatively low cost. In this respect HF radar systems have considerable advantages over in-situ measurements. The accuracy of remote observations does however still not match the quality of in-situ measurements. HF radar transmits electromagnetic (EM) waves in the frequency band between 3-30MHz. The EM wave is reflected by the roughness of the sea surface. The backscattered signal contains information of ocean surface currents and wave heights. In Gurgel et al. (1999), details of the principle of HF radar are given.

Nowadays, HF radars are gaining popularity. They have been deployed in a wide range of coastal environments and provide real time current and wave data over large areas. The data has been used among others to calibrate and validate models (Mau et al. 2007), analyze the spatial and temporal characteristics of surface currents (Cosoli et al., 2012), study the error of radar measured surface currents (Hubbard et al. 2013), or to assimilate real time data into models for marine forecasts (Yu et al., 2012). The application of such systems for early warning of tsunamis is also gaining ground (Lipa et al., 2006).

In the framework of the SPLASH project, a cooperation between the Research and Technology Centre Westcoast and the Yantai Institute of Coastal Zone Research, a WERA system manufactured by Helzel Messtechnik was deployed (Helzel et al., 2006). The system comprises of antenna arrays installed at two

locations on the coast of the Yellow Sea near Yantai, China. The HF radar forms part of a marine now-casting system currently under development for the north coast of the Shandong Peninsula. To assess the effectiveness of the HF radar for measuring current velocities a bottom-mounted ADCP was deployed within the radar coverage area. Results of the assessment are presented in the paper. The radar measurements were also used to identify the main driving mechanisms of the currents off the coast of Yantai. Spectral and harmonic analysis as well as low pass filters were applied to the data. The characteristics of surface current in different frequency domains are discussed with respect to tidal and long period currents as well as the correlation between surface current and wind.

2 DATA

The HF radar system installed near Yantai consists of two stations located at CAU1 and CAU2 as shown in Figure 1. The distance between the two stations is about 9 km. The frequency of the transmitted EM wave is 26.27 MHz, which means that the range of the radar can be up to about 40 km. The bandwidth is 100 KHz. Each station measures radial currents which are combined to obtain the currents in east-west and north-south direction. The velocity vectors are interpolated onto a regular grid of 500m×500m resolution (Figure 1). From July 22 to August 22, 2013 the HF radar recorded surface currents at an integration time of about 16 min and output interval of 20 min. Current records with geometric dilution of precision (GDOP) of more than 5 and a signal to noise ratio below 1.5 were excluded. Due to the ongoing constructions near CAU2 the echo reception from northwest was disturbed resulting in a reduction of the valid coverage area. The coverage of valid data is shown as black patch in Figure 1.

To assess the accuracy of the radar for measuring current velocities a 600 KHz acoustic Doppler current profiler (ADCP) from RD Instruments was deployed bottom mounted in the south of the radar coverage area (Figure 1). The water depth at the deployment site is about 17 m. The vertical resolution (bin size) of the ADCP is 0.5 m. Records are stored every 30 minutes representing the average of 30 measurements within the recording interval. Wind data was also considered in the analysis. The data was extracted from the global model GME of the German Weather Service (DWD) which has a spatial resolution of 30 km and stores the output every three hours (Majewski et al., 2002). Wind of 12 grid points of the GME near the radar domain was averaged to one time series to represent the local wind.

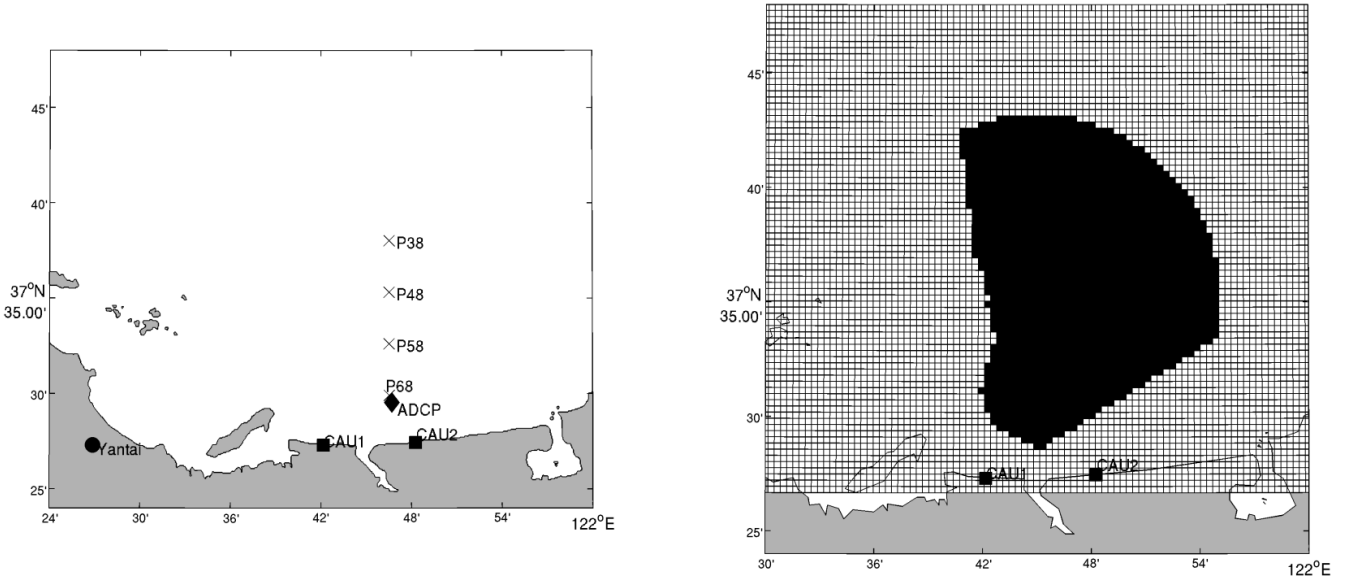


Figure 1. Left: study area near the city of Yantai, in the north coast of Shandong Peninsula, China; location of the two HF radar stations CAU1 and CAU2 denoted by black squares; location of the ADCP denoted by black diamond, position of four points within the radar domain taken in the analysis denoted by black x (P38, P48, P58 and P68 from north to south). Right: 500m×500m grid of the HF radar and coverage of valid measured current data.

3 ASSESSMENT OF THE ACCURACY OF THE HF RADAR

The surface currents observed by the HF radar were compared to the measurements from the bottom mounted upwards looking ADCP. Both devices measure current velocities however in different spatial and temporal domains. The radar data at one grid point represents an average over the horizontal grid cell, while the ADCP measures currents at a point location averaged over several vertical layers. Due to side lobe effects there is considerable noise in the ADCP data close to the free surface. Therefore in this study values at a layer located 1.5 m below the sea surface were used.

Figure 2 shows time series of the comparisons of the east and north components measured by the two instruments. Generally both components of the radar follow the trend of the ADCP measurements, while in the second half of the measuring period the east component shows a better agreement. The agreement was quantified by means of root mean square deviation (RMSD) and correlation coefficients between the time series measured by the instruments. The results are summarized in Table 1. To eliminate the influence of local variability, low pass filters were used to remove higher frequency currents before repeating the assessments. Cutoff frequencies of 3, 25 and 48 hours were chosen. The main tidal frequencies in the area are semidiurnal and diurnal. Removing frequencies below 25 hours therefore means filtering out major tidal currents.

In general, there is better agreement in terms of the east component (U) than for the north component (V). Only for the cut-off of 48h the correlation is lower for the east component (U). RMSD values decrease with increasing cut-off frequency values. That means that for short variations of the surface currents the discrepancies between the two devices are higher while for longer term trends there is good agreement. The RMSD values resulted always below 10 cm/s. The correlation of north component of long-period current is up to 0.84 if the locally dynamic current is removed.

The discrepancies between the measured values might be related to the generally low magnitude of the currents (below 0.3 m/s) and the different spatial and temporal averaging schemes. Other sources of uncertainty are surface waves and atmospheric effects. Figure 2 shows that the differences change in time which is an indication of the influence of variable wave conditions and air characteristics. The sampling frequency of the ADCP is 0.05 Hz and orbital velocities of higher frequency wind waves can induce noise to the currents measured close to the sea surface. On the side of the radar the accuracy is affected by reflections at the ionosphere which increases the background noise and by increased air humidity which disturbs the transmitted and echoed signal (Helzel et al., 2010). Still there is good agreement between the measurements in certain bands of frequency. Therefore we think that the HF radar can provide reasonable free surface currents and it is useful to investigate the main features of the currents over large areas.

Table 1. Overview of the discrepancies between free surface currents measured by the two instruments

| Scheme | U (east) | | V (north) | |
|--------------|-------------|------------|-------------|------------|
| | Correlation | RMSD [m/s] | Correlation | RMSD [m/s] |
| Raw data | 0.69 | 0.08 | 0.45 | 0.09 |
| Cut-off 3h | 0.76 | 0.06 | 0.49 | 0.09 |
| Cut-off 25h | 0.80 | 0.04 | 0.55 | 0.06 |
| Cut-off 48 h | 0.65 | 0.029 | 0.84 | 0.04 |

4 METHODS OF ANALYSIS

The currents in the area are induced primarily by tides, earth rotation, winds and sea water density distribution. Currents are also driven by large scale currents outside the observed area. To distinguish the different influences of these forces spectrum analysis was performed. As ocean circulations move within the rotating earth system, instead of component spectrum analysis, rotary spectrum analysis was used (Gonella, 1972). In rotary spectrum analysis the power density is resolved with respect to the angular velocity of the current vectors. By definition counterclockwise rotation is positive while clockwise rotation is denoted by negative values. Harmonic analysis of tidal currents was also carried out. As a result of harmonic analysis tidal ellipses, consisting of major axis, minor axis and orientation, were determined for the main tidal constituents. The analysis was only performed for data with a signal to noise ratio above one. The frequency of inertial currents in the area (37.8°N) results equal to 1.26 cpd (circle per day).

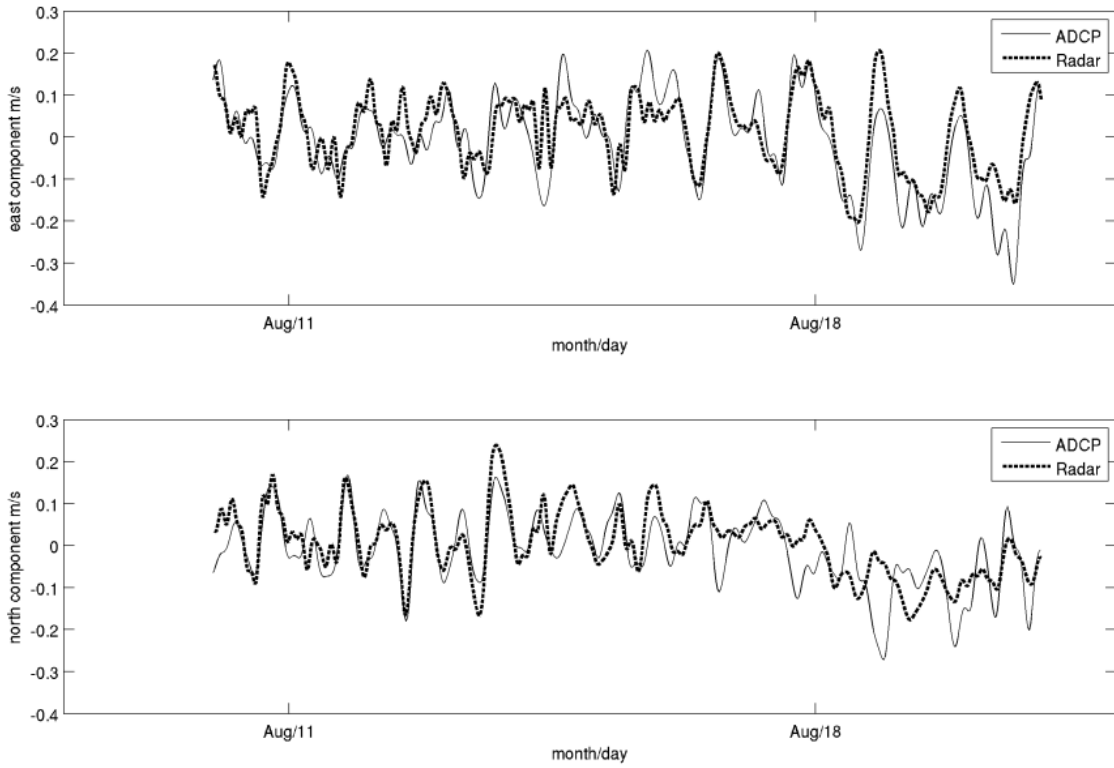


Figure 2. Comparison of time series of free currents (low pass filtered, cut-off time is 3 hours) from ADCP (solid lines) and HF radar (dotted lines) for the east component (upper plot) and north component (lower plot). For clarity, the results are shown only for the period August 10 to 20, 2013.

5 RESULTS AND DISCUSSIONS

5.1 Rotary spectrum analysis

To obtain the representation of the variability of surface currents from offshore towards the coast, rotary spectrum analysis was performed for the radar data at four grid points (p38, p48, p58 and p68) as shown in Figure 1. Figure 3 shows the rotary spectrum of the surface current at the four locations. Clockwise rotation is plotted in dotted line and counterclockwise rotation in solid line. The energy of surface currents focuses in the frequency lower than 2 cpd. The strong tidal influence within the area becomes obvious. Diurnal and semidiurnal components (K1, M2 and O1) dominate the local tidal surface currents.

Considering the four grid points, current energy decreases from offshore towards the coast. The offshore most location P38 has the strongest values and the onshore location P68 the lowest ones. At P38 the highest energy peak appears close to zero rotational frequency which means that there is a comparatively strong current of constant direction. This effect decreases towards the coast. The next distinct energy peaks appear around the tidal frequencies K1 (~ 1 cpd) and O1 (0.93 cpd). At the local inertial frequency 1.26 cpd there is another concentration of energy in clockwise rotation. The influence of the M2 (1.93 cpd) tidal frequency is also visible with about half of the energy of the diurnal components. For frequencies below 0.5 cpd, there are some smaller energy peaks which may be related to wind influence.

A general understanding of the surface current patterns in the area can be obtained on the basis of the results. Tides with predominant diurnal components seem to be the major driving forces. Since the local inertial frequency is not close to any tidal frequency, the presence of considerable inertial currents could also be distinguished. The source of the observed inertial movements could not be clearly identified as the inertial oscillations appear after the decay of the driving force. There are also currents of longer period which are possibly related to wind effects. Apart from the oscillatory movements a distinct constant current (of frequency 0) is also present in locations further offshore. Results of a more detailed analysis for the principal components of the currents are presented below.

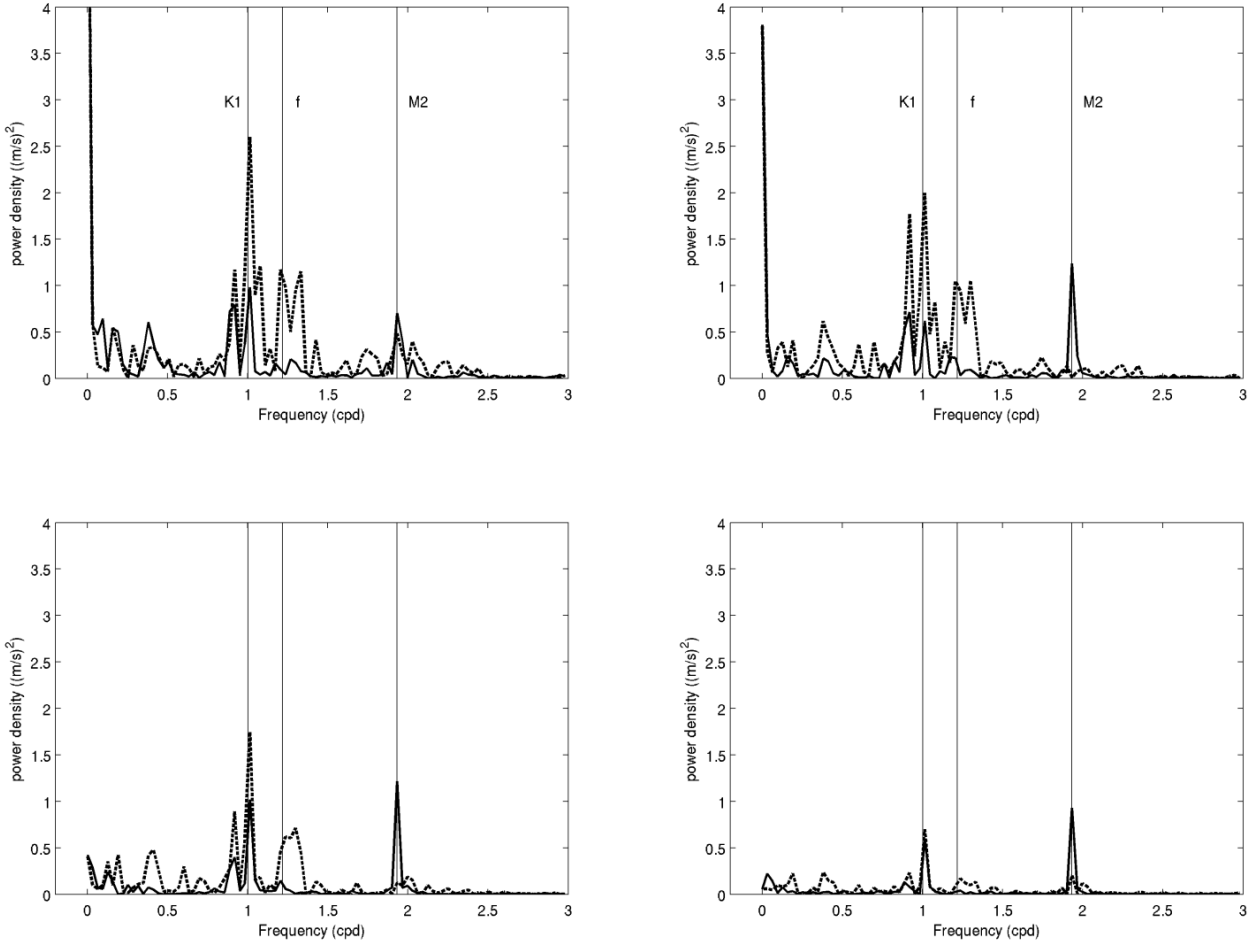


Figure 3. Rotary spectrum analysis at four points (P38, P48, P58 and P68 as shown in Figure 1). Clockwise spectrum and counterclockwise spectrums are indicated respectively by dotted and solid lines.

5.2 Harmonic analysis of surface currents

Harmonic analysis of tidal currents was performed using the Matlab toolbox T_Tide by Pawlowicz et al. (2002). The analysis was done for every grid point of the radar grid containing valid data. The spatial distribution of the tidal ellipse of the main diurnal component K1 and main semi-diurnal M2 is shown in Figure 4.

K1 has the largest energy among the relevant tidal components (cf. Figure 3); the amplitude of K1 can be up to 0.15 m/s in the upper part of the radar domain, and it decreases to about 0.07 m/s closer to the coast. The tidal K1 currents rotate in clockwise direction at all grid points. The K1 ellipses in the western part are rather flat indicating that the currents normal to the coastline are small compared to the along-shore currents. In the eastern part the K1 ellipses are more round and the major axes are orientated in south west - north east direction.

M2 is the second dominating tidal component. The amplitudes of M2 range from 0.12 m/s in the upper part of the radar domain to 0.05 m/s at the southern most point. The currents rotate counterclockwise in the southern and central part and clockwise in the north and east of the radar domain. The M2 current is influenced by two tidal amphidromic systems (Sun, 1994) resulting in a divergence in the middle of the radar domain.

5.3 Long period currents

Figure 5 shows contours of the two current vectors (U and V) after low pass filtering with a 15 day cut off. It was found that these currents are roughly similar to the average currents of the whole recorded period. The quasi-constant currents flow approximately along the coastline. The highest value is about 0.22 m/s at the location of $121^{\circ}45.0'E$, $37^{\circ}38.4'N$; the current velocity decreases from this point towards offshore and towards the coast. The north component of the current is smaller and increases from 0 to 0.07 m/s from west to the east part of the radar domain.

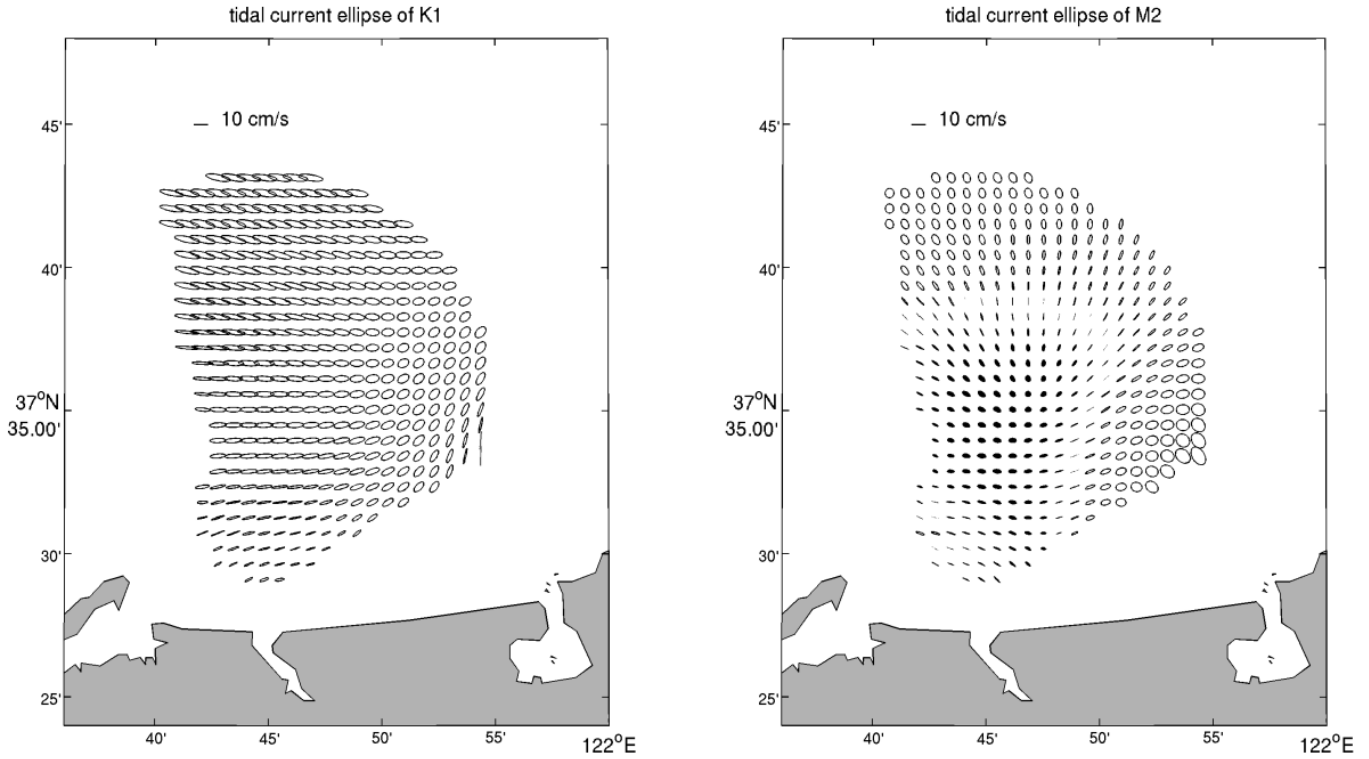


Figure 4. The tidal ellipses of two main tidal constituents, K1 (left) and M2 (right). The ellipses drawn in lines indicate clockwise rotation, the patched ellipses indicate counterclockwise rotation.

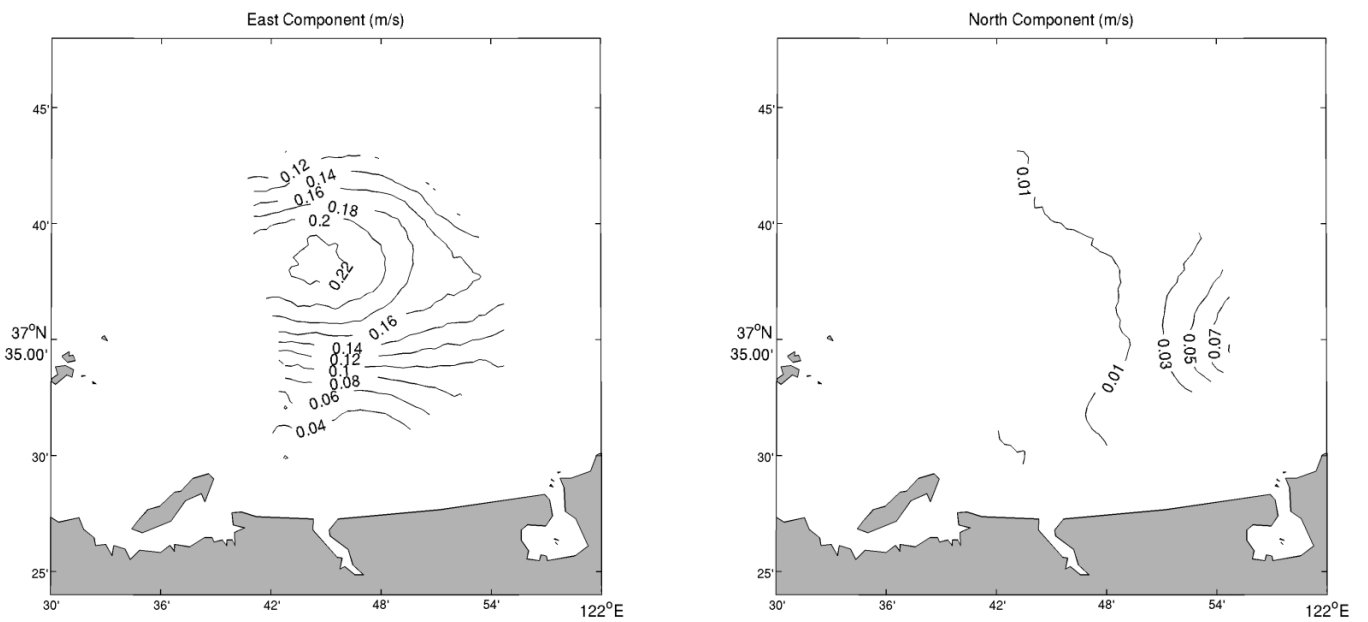


Figure 5. The low pass filtered current (cut-off period is 15 days) along the east (left) and north (right) directions.

Su (2005) also pointed out the existence of a longshore current in the north coast of Shandong Peninsula, as part of the coastal current system in the East China Sea. The dominating wind direction in summer in this region is southerly. Thus it is unlikely for local winds alone to induce such long period eastward currents. Another driving mechanism for the longshore current might be density differences between the Bohai Sea and Yellow Sea. With water depths usually less than 20 m the western part of the Bohai Sea is shallower than the northern Yellow Sea. This together with water temperature differences between the two seas (Chen et al., 1992), results in water level gradients and longshore currents from the Bohai Sea towards the Yellow Sea. The mechanism of the longshore current will be studied by more current observation and model simulations in following studies.

5.4 Correlation between local wind and free surface currents

From the spectral analysis of the surface currents, peaks between 0 and 0.5 cpd can be identified. The rotary spectrum of local wind (Figure 6) shows there are several peaks in the band between 0 and 0.5 cpd, and that the energy is especially high over the frequencies lower than 0.1 cpd; there is a minor peak exactly at the frequency of 1 cpd which most probably is caused by land-sea breeze. A low pass filter with cut-off period of 50 hours was used to remove the frequencies higher than 0.5 cpd of surface current along both east and north direction on each grid points.

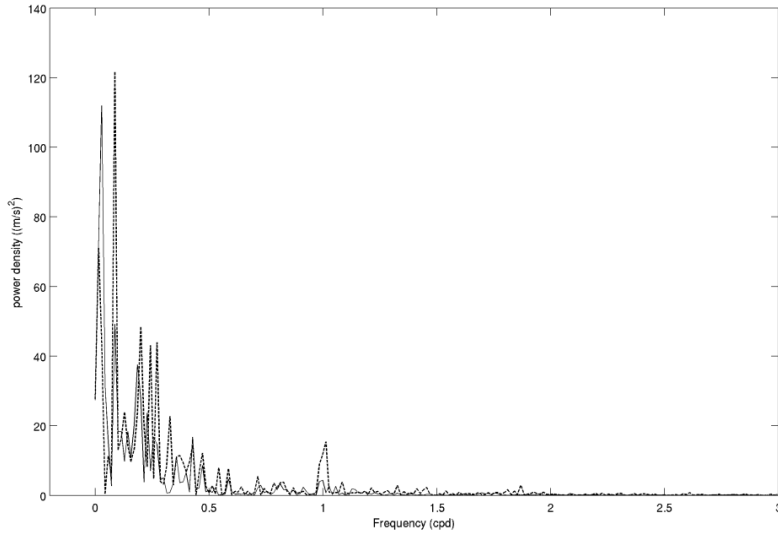


Figure 6. Rotary spectrum of wind in the period of July, August and September, 2013. Solid and dotted lines denote respectively counterclockwise and clockwise rotations.

To determine the relation between the surface currents and local wind, correlation coefficients were computed. The resulting values over the radar domain are shown in Figure 7. It can be seen that correlation coefficients in east direction range mainly from 0.2 to 0.6; there is an area of low correlation coefficients, with values below 0.2, in the centre of the radar domain; correlation coefficients increase to 0.6 in the northern and southern parts; the correlation can be up to 0.7 at a small area closer to the coast. The correlation between wind and current in north direction range from 0.1 to 0.8; the area in the southern part of the domain has the largest correlation up to about 0.8; the correlation decrease in a very regular way from west to east with values varying from 0.7 to 0.1. Comparisons between Figures 5 and 7 show that in places where the long period currents are stronger the correlation between wind and current is weaker. This demonstrates that the density difference is an important factor for summer currents.

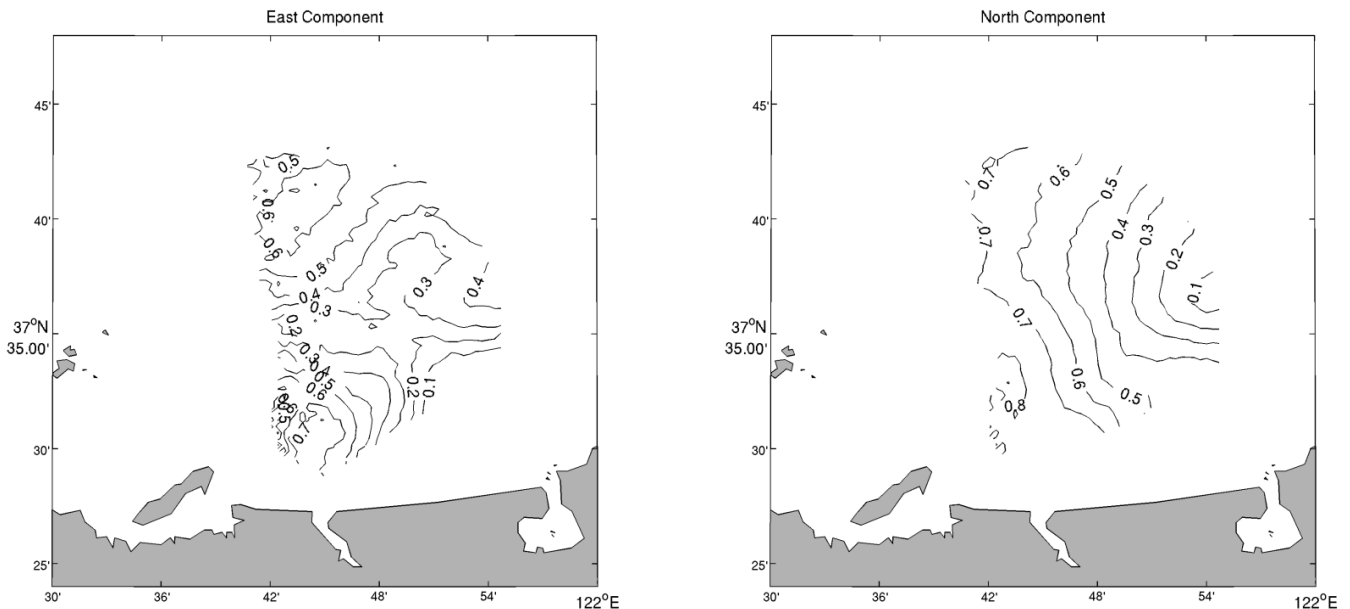


Figure 7. Correlation between low pass filtered wind and surface currents (cut-off time is 50 hour).

6 CONCLUSIONS

Results of the investigation of the effectiveness of the land based HF radar for measurement of free surface current velocities near Yantai in China are presented. The discrepancies in terms of RMSD values between the HF radar and ADCP resulted below 0.1m/s. The general variation of tidal currents and longer term trends, as recorded by the ADCP, were also detected by the radar even though there are periods of considerable deviation. The discrepancies between the current records from the two instruments might be related to the different spatial and temporal integration. Other sources might be related to the difficulty in removing the influence of electronic noise from the HF radar data and wave orbital velocities from the ADCP data. The radar data was used to obtain the main patterns of current velocity in the area. Different techniques were adopted to improve the understanding about the characteristic patterns of surface currents. Spectrum, harmonic and correlation analysis lead to the identification of the main features. Within the period of analysis from July to August, 2013, a low frequency (quasi constant) current with magnitudes of up to about 0.2 m/s flowing alongshore was identified. The currents are considered to be a part of a large-scale density induced circulation between the Bohai Sea and Yellow Sea. It was found that tidal and longshore currents are of similar magnitude and the energy from diurnal components is approximately twice the one from semi-diurnal currents. The local wind can bring noticeable effect on the currents, especially in places where the low frequency current is weak. The findings are in good agreement with previous studies and the applicability of the HF radar was confirmed. Additional analyses of the local current patterns are currently underway. The data, in quasi-real time, is being used for the development of flow and wave models and being integrated within a nowcasting modeling system covering parts of the Shandong Peninsula.

ACKNOWLEDGMENTS

The authors wish to thank the German Ministry of Education and Research (BMBF) for the funding of the project SPLASH (Funding number 03F0632A). The discussions of radar data processing with experts from Helzel Messtechnik GmbH, Kaltenkirchen are appreciated. We are also grateful to the German Weather Service (DWD) for providing the wind data from the global model GME.

REFERENCES

- Chen, D., Sun, X., and Pu, Y. (1992). Marine atlas of Bohai sea, Yellow sea and East China sea-Hydrology, Ocean Press.
- Cosoli, S., Gačić, M., and Mazzoldi, A. (2012). Surface current variability and wind influence in the northeastern Adriatic Sea as observed from high-frequency (HF) radar measurements. *Continental Shelf Research*, 33, 1-13.
- Gonella, J. (1972, December). A rotary-component method for analysing meteorological and oceanographic vector time series. In *Deep Sea Research and Oceanographic Abstracts* (Vol. 19, No. 12, pp. 833-846). Elsevier.
- Gurgel, K. W., Essen, H. H., and Kingsley, S. P. (1999). High-frequency radars: physical limitations and recent developments. *Coastal Engineering*, 37(3), 201-218.
- Helzel, T., Kniephoff, M., and Petersen, L. (2006, May). WERA: remote ocean sensing for current, wave and wind direction. In *Proc US/EU-Baltic Int Symposium* (pp. 23-25).
- Helzel, T., Kniephoff, M., and Petersen, L. (2010). Oceanography radar system WERA: features, accuracy, reliability and limitations. *Turkish J. Elect. Eng. Comput. Sci.*, 18(3), 389-397.
- Hubbard, M., Barrick, D., Garfield, N., Pettigrew, J., Ohlmann, C., and Gough, M. (2013). A new method for estimating high-frequency radar error using data from Central San Francisco Bay. *Ocean Science Journal*, 48(1), 105-116.
- Lipa, B. J., Barrick, D. E., Bourg, J., and Nyden, B. B. (2006). HF radar detection of tsunamis. *Journal of Oceanography*, 62(5), 705-716.
- Majewski, D., Liermann, D., Prohl, P., Ritter, B., Buchhold, M., Hanisch, T., and Baumgardner, J. (2002). The operational global icosahedral-hexagonal gridpoint model GME: Description and high-resolution tests. *Monthly Weather Review*, 130(2), 319-338.
- Mau, J. C., Wang, D. P., Ullman, D. S., and Codiga, D. L. (2007). Comparison of observed (HF radar, ADCP) and model barotropic tidal currents in the New York Bight and Block Island Sound. *Estuarine, Coastal and Shelf Science*, 72(1), 129-137.
- Sun, C., Wang, X., Zhao, K. (1994). Simulation of tidal current off the north coast of Yantai (in Chinese). *Periodical of Ocean University of Qingdao*, S1.
- Su, J. (2005). *Coastal hydrology of China* (in Chinese), Ocean Press.
- Pawlowicz, R., Beardsley, B., and Lentz, S. (2002). Classical tidal harmonic analysis including error estimates in MATLAB using T_TIDE. *Computers & Geosciences*, 28(8), 929-937.
- Yu, P., Kurapov, A. L., Egbert, G. D., Allen, J. S., and Kosro, P. M. (2012). Variational assimilation of HF radar surface currents in a coastal ocean model off Oregon. *Ocean Modelling*, 49, 86-104.